Global and Planetary Change 210 (2022) 103755

Contents lists available at ScienceDirect

Global and Planetary Change

journal homepage: www.elsevier.com/locate/gloplacha

Ice sheet decline and rising atmospheric CO_2 control AMOC sensitivity to deglacial meltwater discharge

Yuchen Sun [a], Gregor Knorr [a,*], Xu Zhang [a,b], Lev Tarasov [c], Stephen Barker [d], Martin Werner [a], Gerrit Lohmann [a,e]

[a] Alfred Wegener Institute, Helmholtz Centre for Polar and Marine Research, Bussestr. 24, D-27570 Bremerhaven, Germany
[b] State Key Laboratory of Tibetan Plateau Earth System, Resources and Environment (TPESRE), Chinese Academy of Sciences (CAS), Beijing, China
[c] Dept. of Physics and Physical Oceanography, Memorial University of Newfoundland, St. John's, NL, Canada
[d] School of Earth and Environmental Sciences, Cardiff University, Wales, UK
[e] University of Bremen, 28359 Bremen, Germany

ARTICLE INFO

Editor: Howard Falcon-Lang

Keywords:
Deglaciation
Termination 1
AOGCM
GLAC-1D
Last Glacial Maximum
Heinrich Stadial
Bølling/Allerød interstadial
Abrupt climate change
AMOC

ABSTRACT

The last deglaciation was characterized by a sequence of abrupt climate events thought to be linked to rapid changes in Atlantic meridional overturning circulation (AMOC). The sequence includes a weakening of the AMOC after the Last Glacial Maximum (LGM) during Heinrich Stadial 1 (HS1), which ends with an abrupt AMOC amplification at the transition to the Bølling/Allerød (B/A). This transition occurs despite persistent deglacial meltwater fluxes that counteract vigorous North Atlantic deep-water formation. Using the Earth system model COSMOS with a range of deglacial boundary conditions and reconstructed deglacial meltwater fluxes, we show that deglacial CO_2 rise and ice sheet decline modulate the sensitivity of the AMOC to these fluxes. While declining ice sheets increase the sensitivity, increasing atmospheric CO_2 levels tend to counteract this effect. Therefore, the occurrence of a weaker HS1 AMOC and an abrupt AMOC increase in the presence of meltwater, might be explained by these effects, as an alternative to or in combination with changes in the magnitude or routing of meltwater discharge.

1. Introduction

Glacial to interglacial changes represent the largest global-scale climate variations during the Quaternary. These glacial terminations are characterized by a high degree of internal non-linearity since their origin has been linked to a relatively modest gradual external insolation forcing as compared with equivalent insolation changes that do not result in termination (Imbrie et al., 1993; Raymo, 1997). While there is an increasing consensus that abrupt changes in the Atlantic Meridional Overturning Circulation (AMOC), including millennial-scale oscillations (Böhm et al., 2015; Deaney et al., 2017; Venz et al., 1999; Barker et al., 2011), might have played a fundamental role in determining the shape and rapidity of deglaciation (e.g. Denton et al., 2010; Barker and Knorr, 2021), the specific sequence of climatic events during Termination I has led to much debate regarding a mechanistic understanding of terminations in general. The abrupt AMOC amplification at the beginning of the Bølling/Allerød (B/A) interstadial after a phase of reduced Atlantic overturning during Heinrich Stadial 1 (HS1) has especially challenged our understanding of abrupt climate changes in face of progressive ice sheet disintegration. Explanations generally involve changes in AMOC stability (e.g., Stocker, 2000; Lohmann and Schulz, 2000; Knorr and Lohmann, 2003; Ganopolski and Roche, 2009) or spatiotemporal variations in meltwater input to the North Atlantic (e.g., Liu et al., 2009; Menviel et al., 2011) midway through the last deglaciation.

For example an abrupt AMOC strengthening in deglacial model experiments (He et al., 2013; Liu et al., 2009; Menviel et al., 2011) has been simulated by a cessation of North Atlantic meltwater discharge. However other model investigations suggested that abrupt AMOC transitions can be directly triggered by gradual global warming (Knorr and Lohmann, 2007; Barker and Knorr, 2007; Dima et al., 2018). Furthermore, it has been demonstrated that atmospheric CO_2 and ice sheet height can influence the AMOC strength (Galbraith and de Lavergne, 2019; Oka et al., 2012; Muglia and Schmittner, 2015; Klockmann et al., 2016; Sherriff-Tadano et al., 2018) and the occurrence of abrupt climate changes (Zhang et al., 2014, 2017; Banderas et al., 2015; Klockmann et al., 2018). More specifically a recent fully coupled

* Corresponding author.
E-mail address: gregor.knorr@awi.de (G. Knorr).

https://doi.org/10.1016/j.gloplacha.2022.103755
Received 18 December 2020; Received in revised form 6 December 2021; Accepted 29 January 2022
Available online 9 February 2022

atmosphere-ocean general circulation model (AOGCM) study (Obase and Abe-Ouchi, 2019) has shown that an abrupt AMOC amplification at the B/A transition could occur without reduction or cessation of glacial meltwater to the North Atlantic. In this scenario gradual deglacial warming weakens stratification in the North Atlantic and causes a rapid retreat of sea ice and initiation of deep-water formation. However, in spite of simulating a B/A-like event, the initial deglacial AMOC reduction after the Last Glacial Maximum (LGM, ~21 ka BP) is not captured in Obase and Abe-Ouchi (2019). In this context, the application of fixed LGM ice sheet conditions can be critical, as a Northern Hemisphere ice sheet decline might have altered the stability properties of the AMOC (Zhang et al., 2014) and may have weakened the deglacial AMOC (Zhu et al., 2014).

Here we investigate changes in the AMOC with respect to key

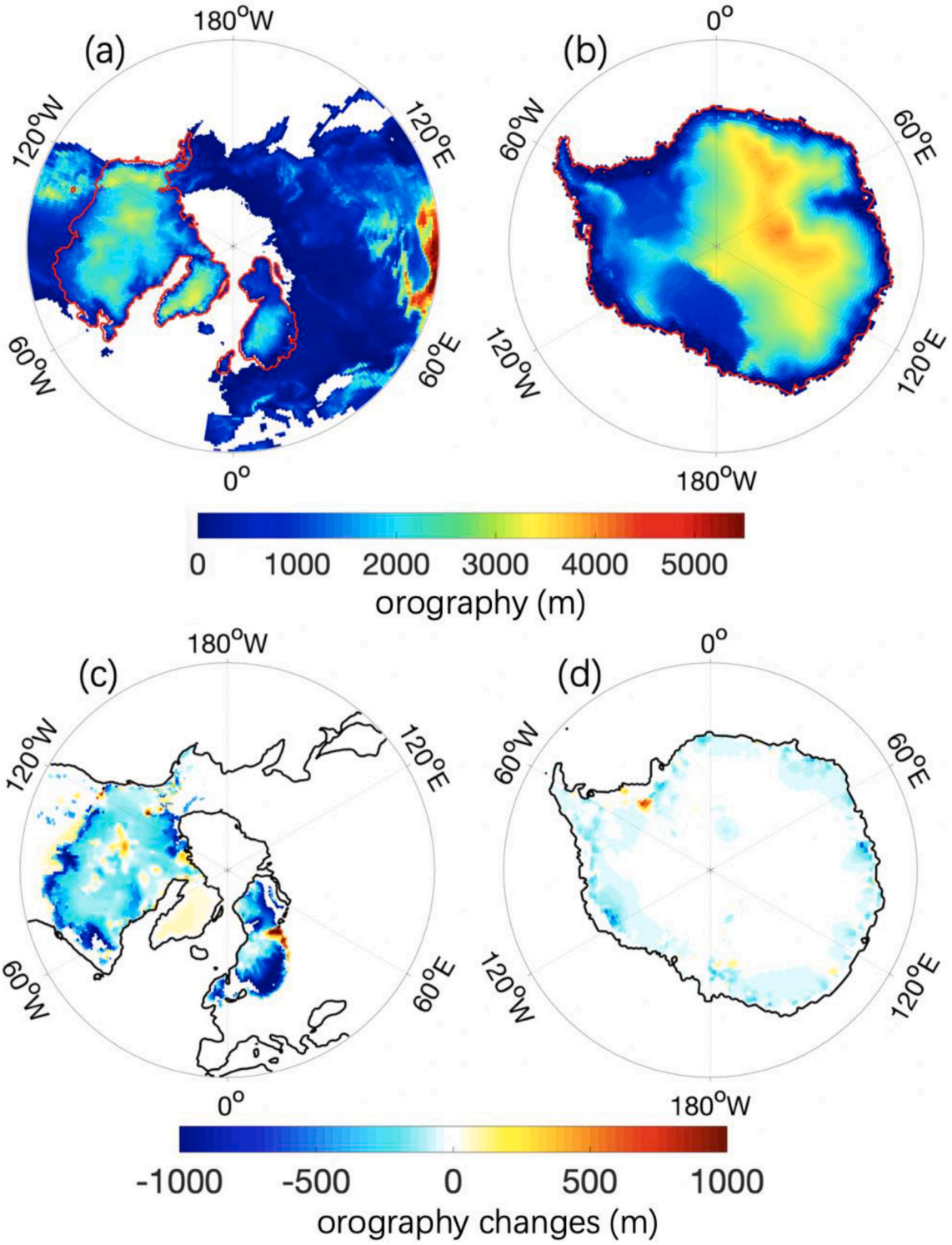

Fig. 1. Orography (m) at16 ka BP from GLAC-1D in a) the Northern Hemisphere and b) the Southern Hemisphere. The ice sheet extent is indicated by red lines. In panels c) and d) the orography anomalies between LGM and 16 ka are shown. The black lines in panels c) and d) represent the coastline at the LGM. (For interpretation of the references to colour in this figure legend, the reader is referred to the web version of this article.)

forcings and boundary conditions during deglaciation including changes in atmospheric CO_2 concentration and continental ice sheets by a suite of simulations with the fully-coupled ocean-atmosphere-sea ice-land surface model COSMOS. Ice Sheet changes include associated deglacial meltwater and iceberg fluxes (MWF) based on the state-of-the art GLAC-1D reconstruction (Tarasov et al., 2012). In particular we show that the decline of Northern Hemisphere ice sheets increases the sensitivity of the AMOC to North Atlantic meltwater discharge while rising atmospheric CO_2 concentrations tend to counteract this effect. Therefore, the climate system, as represented by COSMOS, can to first order undergo the HS1 to B/A oscillation without changes in surface meltwater routing nor changes in the net meltwater discharge from the ice sheets.

2. Methods

2.1. Model description

We use the fully-coupled ocean-atmosphere-sea ice-land surface model COSMOS (Jungclaus et al., 2006). The ocean component MPI-OM (Marsland et al., 2003) including a dynamic sea-ice model (Hibler III, 1979) and has a formal horizontal resolution of GR30 (3° × 1.8°), with 40 uneven vertical layers. The MPI-OM set-up has a bipolar orthogonal spherical coordinate system, where the poles are placed over Greenland and Antarctica, respectively. The atmospheric component ECHAM5 (Roeckner et al., 2003) runs at a horizontal resolution of ~3.75° × 3.75° with 19 vertical levels and is complemented by the land surface scheme JSBACH (Raddatz et al., 2007) including a dynamical vegetation module (Brovkin et al., 2009). The climate model has already been used to simulate the past millennium (Jungclaus et al., 2010), the Miocene warm climate (Knorr et al., 2011; Knorr and Lohmann, 2014; Huang et al., 2017; Hossain et al., 2020), the Pliocene (Stepanek et al., 2020), the internal variability of the climate system (Wei et al., 2012), Holocene variability (Wei and Lohmann, 2012), the Last Glacial Maximum (LGM) climate (Zhang et al., 2013; Simon et al., 2015; Abelmann et al., 2015) and glacial millennial-scale variability (Gong et al., 2013; Knorr et al., 2021; Zhang et al., 2021).

2.2. GLAC-1D

The orography used in our investigations (Fig. 1), is based on the GLAC-1D ice sheet reconstruction (Tarasov et al., 2012; Briggs et al., 2014; Tarasov et al., 2014). All of the GLAC-1D ice-sheet components employ dynamical ice sheet models that have been constrained with multiple proxy indicators and modern observations. In this study, a distribution of freshwater due to melting and calving is self-consistently implemented in our COSMOS model set-up to study abrupt climate changes during the last deglaciation. The GLAC-1D reconstruction contains not only the extent and thickness of the ice sheet, but also a surface drainage pointer field and approximate partition of solid and liquid discharge at the ice sheet margins. We use this information to distribute the MWF to the corresponding coastal areas (Fig. 2). The magnitude of the global MWF from the ice sheets is calculated by ice volume changes based on 100 year intervals, representing the net MWF. The main contribution to the global signal is the meltwater discharge in the North Atlantic/Arctic catchment area (Fig. 3). Because of the lack of an explicit iceberg model, we impose the calving fraction of discharge from Northern Hemisphere ice sheets provided by GLAC-1D into the ice-rafted debris (IRD) belt (40°N–55°N, 45°W–20°W; Hemming, 2004) of the North Atlantic. In the following the notation MWF refers to the combined flux associated with melting and calving to represent the analogue contribution to meltwater perturbations in hosing experiments. Please note that this does not mean that our model approach ignores precipitation minus evaporation which is inherently represented by the hydrological cycle within COSMOS.

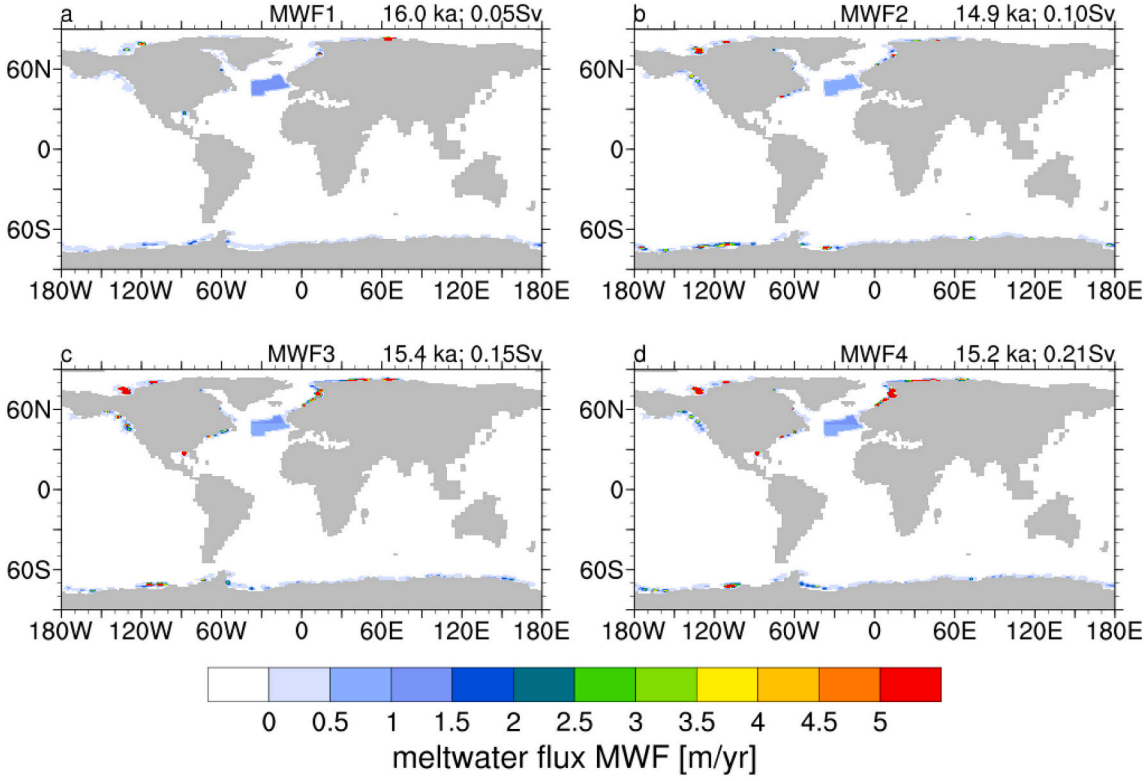

Fig. 2. Map of meltwater discharge (MWF, meltwater flux in m/yr) in the different simulations at a) 16 ka BP, b) 15.4 ka BP, c) 15.2 ka BP, d) 14.9 ka BP. The MWF fields consist of two parts: the melt water part of the glacial ice sheets (located at different coastal regions) and the part due to iceberg melting in the IRD belt of the North Atlantic. The MWF is derived from the GLAC-1D reconstruction.

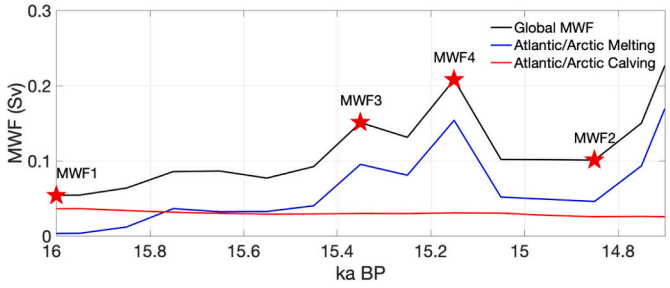

Fig. 3. Temporal evolution of the total global (black) MWF (Sv) and the Atlantic contributions by melting (blue) and calving (red) from GLAC-1D between 16 ka BP and 14.6 ka BP. The red stars correspond to the MWF scenarios 1 to 4 in Fig. 2 and Table 1. (For interpretation of the references to colour in this figure legend, the reader is referred to the web version of this article.)

2.3. Experiments

An overview of experiment characteristics of all simulations in this study are provided in Table 1. Details of the prescribed GLAC-1D orography and deglacial meltwater discharge fields are provided in Table 1 and Figs. 1-3.

Geological evidence suggests the occurrence of meltwater pulses at 19 ka BP (19 ka MWP) (Clark et al., 2004), 17.5 ka BP and 16 ka BP (Bard et al., 2000). Before we perform any experiments with meltwater fluxes, a simulation without meltwater input is conducted as the control state for 16 ka conditions in experiment 16KCTL. The orbital forcing is from Berger (1978) and the atmospheric greenhouse gas concentrations are prescribed according to reconstructions from ice cores (Bereiter et al., 2015; Loulergue et al., 2008; Schilt et al., 2010; Köhler et al., 2017). This simulation is initialized from an LGM simulation, which has been integrated for 4000 years under PMIP3 LGM background conditions (Zhang et al., 2013) representative of the time slice 21 ka BP. The largest ice sheet changes between LGM and 16KCTL take place in the Northern Hemisphere at the margins of the ice sheets, which is most pronounced in the ice sheet height decrease along southern ice sheet segments (Fig. 4c). Based on the 16 ka state we designed a suite of sensitivity experiments to test the impact of different meltwater fluxes on AMOC. The Bering St. is closed in all simulations, a confident aspect of GLAC-1D for this time interval.

According to GLAC-1D, for the 16 ka BP to B/A onset interval, the total amount of global net MWF spans a range between 0.04Sv and 0.21Sv. To assess the potential AMOC changes to a range of meltwater variations in the corresponding time interval, (as well as partially address GLAC-1D chronological uncertainties) we chose four different meltwater discharge configurations (Table 1, Figs. 2, 3) representative of 16 ka (MWF1 in experiment 16K_0.05 with 0.05 Sv), 14.9 ka (MWF2 in experiment 16K_0.1 with 0.10 Sv), 15.4 ka (MWF3 in experiment 16K_0.15 with 0.15 Sv) and 15.2 ka (MWF4 in experiment 16K_0.2 with 0.21 Sv). Additionally, we performed one experiment (16K_0.1_0.2_grad) with a gradual MWF increase to 0.21 Sv in 1000 years based on 16K_0.1.

For comparison with the 16 ka state experiments, we conducted two LGM state hosing experiments that apply the deglacial meltwater discharge pattern according to MWF2 in experiments LGM_0.1 and LGM_0.18. The respective discharge magnitudes in these two LGM experiments are 0.1 Sv and 0.18 Sv, respectively (cf. section 3.3).

The 16 ka and LGM simulations are complemented by three experiments with hybrid boundary conditions that all represent full LGM conditions except a 16 ka ice sheet configuration to disentangle CO_2 and ice-sheet effects. Experiment LGM_16KICE is conducted without any meltwater discharge resulting from ice volume changes. In contrast ice volume changes equivalent to a MWF of 0.1 Sv and 0.15 Sv are distributed by the MWF2 pattern in experiment LGM_16KICE+0.1 and LGM_16KICE+0.15, respectively.

2.4. HS1-B/A transition

The HS1-B/A transition occurred around 14.7 ka BP. According to GLAC-1D, the total amount of MWF at this time is ~0.22 Sv, which is larger than the MWF used in our freshwater sensitivity runs. Depending on the geographic pattern of injection, such a large amount of freshwater could force the AMOC into a weak mode. To return to a strong AMOC mode, other forcing might have played a key role, such as a gradual CO_2 increase (Zhang et al., 2017; Barker et al., 2019). Therefore, we test whether the rise in atmospheric CO_2 concentration can restore the AMOC in the presence of a large amount of MWF. Among our freshwater sensitivity experiments, the experiment MWF4 has the largest freshwater input (0.21Sv), which is close to the amount of freshwater when the BA event occurs in the GLAC-1D reconstruction. A transient experiment (16K_0.21_CO2) mimicking the CO_2 rise into the B/A is conducted to test the CO_2 effect for the AMOC recovery process with the presence of this large MWF.

3. Results

The application of the various boundary conditions (Table 1, Figs. 1-3) reveals three basic types of AMOC trajectories (Fig. 4). The first is a modest AMOC weakening, which occurs in experiments LGM_16KICE and 16KCTL. The second is a relatively strong transient AMOC reduction followed by an abrupt AMOC intensification after several hundreds of

Table 1
This table summarizes experiment characteristics of all simulations in this study.

ID	Boundary Conditions	Initial Conditions	Freshwater Routing	Global Meltwater Magnitude	Atlantic/Arctic Melting	Atlantic/Arctic Calving	Integration of Model Years
16KCTL	16 ka	LGM		0Sv	0Sv	0Sv	1000
16K_0.05	16 ka	LGM	MWF1	0.054Sv	0.004Sv	0.036Sv	1200
16K_0.10	16 ka	LGM	MWF2	0.101Sv	0.046Sv	0.026Sv	1650
16K_0.15	16 ka	LGM	MWF3	0.151Sv	0.095Sv	0.030Sv	2200
16K_0.21	16 ka	LGM	MWF4	0.208Sv	0.154Sv	0.031Sv	3500
16K_0.1_0.2_grad	16 ka	16K_0.10	MWF2	0.101Sv to 0.208Sv	0.046Sv to 0.095Sv	0.026Sv to 0.054Sv	1000
16K_0.21_CO2	16 ka, transient CO_2	model year 2000 in 16K_0.21	MWF4	0.208Sv	0.154Sv	0.031Sv	1400
LGM_16KICE	16 ka ice sheet, LGM CO_2, LGM ORB	LGM		0Sv	0Sv	0Sv	800
LGM_16KICE+0.10	16 ka ice sheet, LGM CO_2, LGM ORB	LGM_16KICE	MWF2	0.101Sv	0.046Sv	0.026Sv	800
LGM_16KICE+0.15	16 ka ice sheet, LGM CO_2, LGM ORB	LGM_16KICE	MWF2	0.151Sv	0.069Sv	0.039Sv	800
LGM_0.10	LGM	LGM	MWF2	0.101Sv	0.046Sv	0.026Sv	800
LGM_0.18	LGM	LGM	MWF2	0.180Sv	0.082Sv	0.046Sv	800

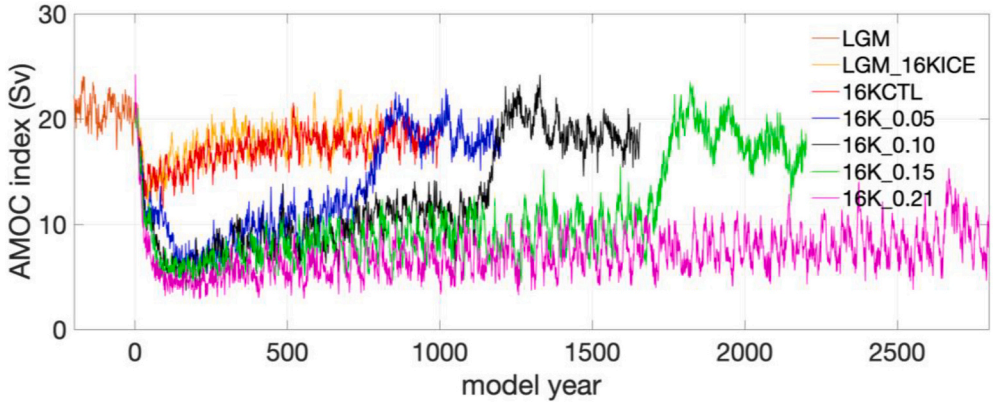

Fig. 4. Time evolution of the AMOC (Sv) defined as the maximum value of the stream function below 500 m in the North Atlantic for different sensitivity experiments (cf. Figs. 2, 3 and Table 1). All experiments are started from experiment LGM at year zero.

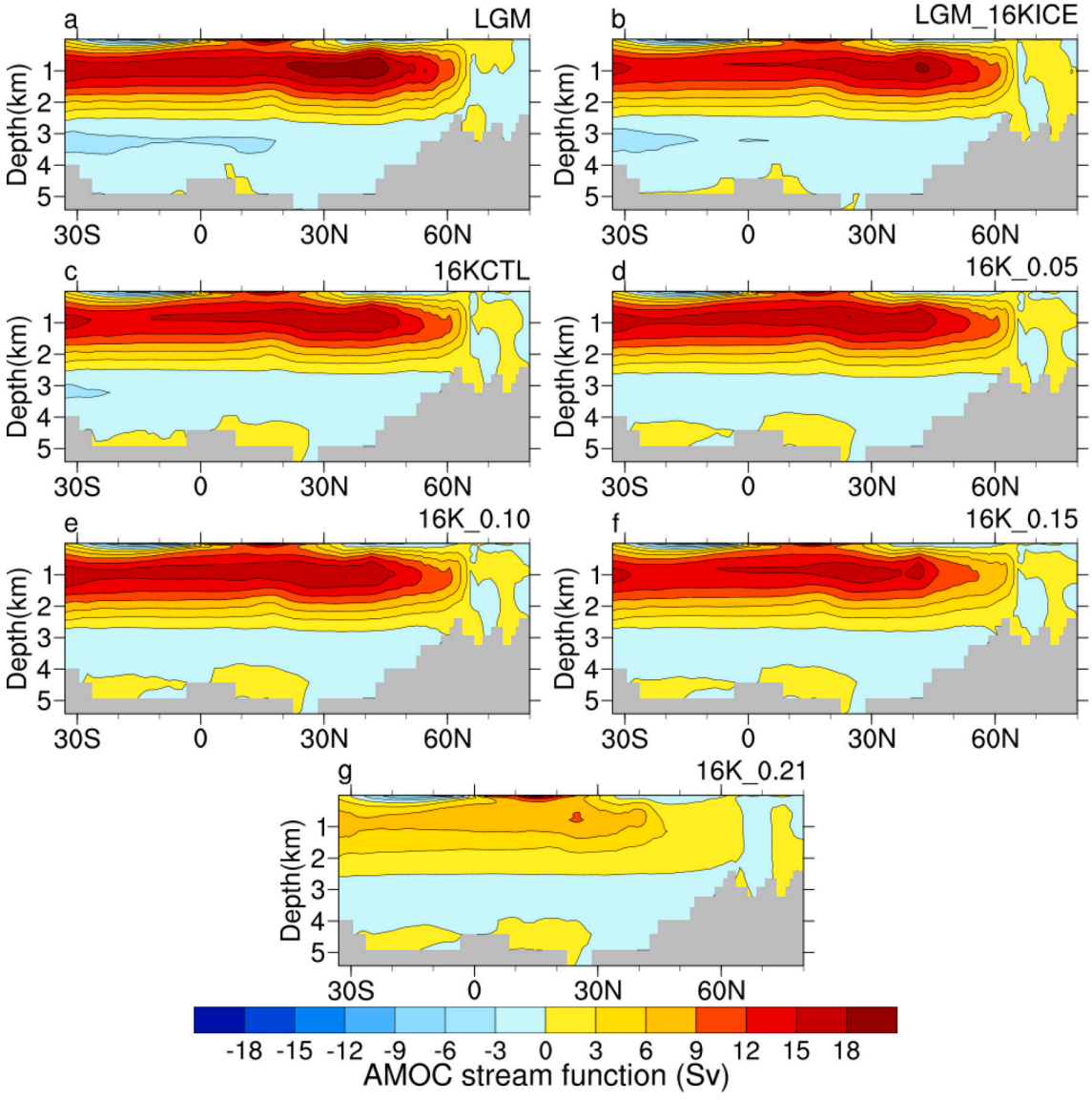

Fig. 5. AMOC (Sv) for the sensitivity experiments in Fig. 4, represented by the average of the last 100 model years. Positive and negative values indicate clockwise and anti-clockwise circulation, respectively.

years under fixed deglacial MWF in experiments 16K_0.05, 16K_0.1, 16K_0.15. The third trajectory is simulated in experiment 16K_0.21, which shows a persistent weak AMOC without a rapid AMOC amplification. In Fig. 5 we show the resulting AMOC states in the different experiments averaged over the last 100 model years of each individual simulation in Fig. 4. All states are characterized by weaker Atlantic overturning than in the base LGM state.

In our 16 ka control simulation (16KCTL) the AMOC stabilizes at ~18 Sv, which is slightly weaker than the LGM state at ~21 Sv. If we maintain the atmospheric CO_2 concentration and the orbital forcing at the level of the LGM state, and only consider the ice-sheet change at 16 ka BP (LGM_16KICE), the AMOC change is very similar to 16KCTL. This suggests that the decrease in ice-sheet height is the main cause of the reduced AMOC in 16KCTL and shows that the 16 ka boundary conditions without any additional forcing (e.g. MWF) are not sufficient to cause the large AMOC decrease inferred for typical HS1 conditions (e.g. McManus et al., 2004). To address the differences that govern the transient AMOC dynamics in the hosing experiments we investigate the mechanism for an abrupt AMOC intensification in section 3.1. Thereafter in section 3.2, we focus on the impact of rising CO_2 on the threshold

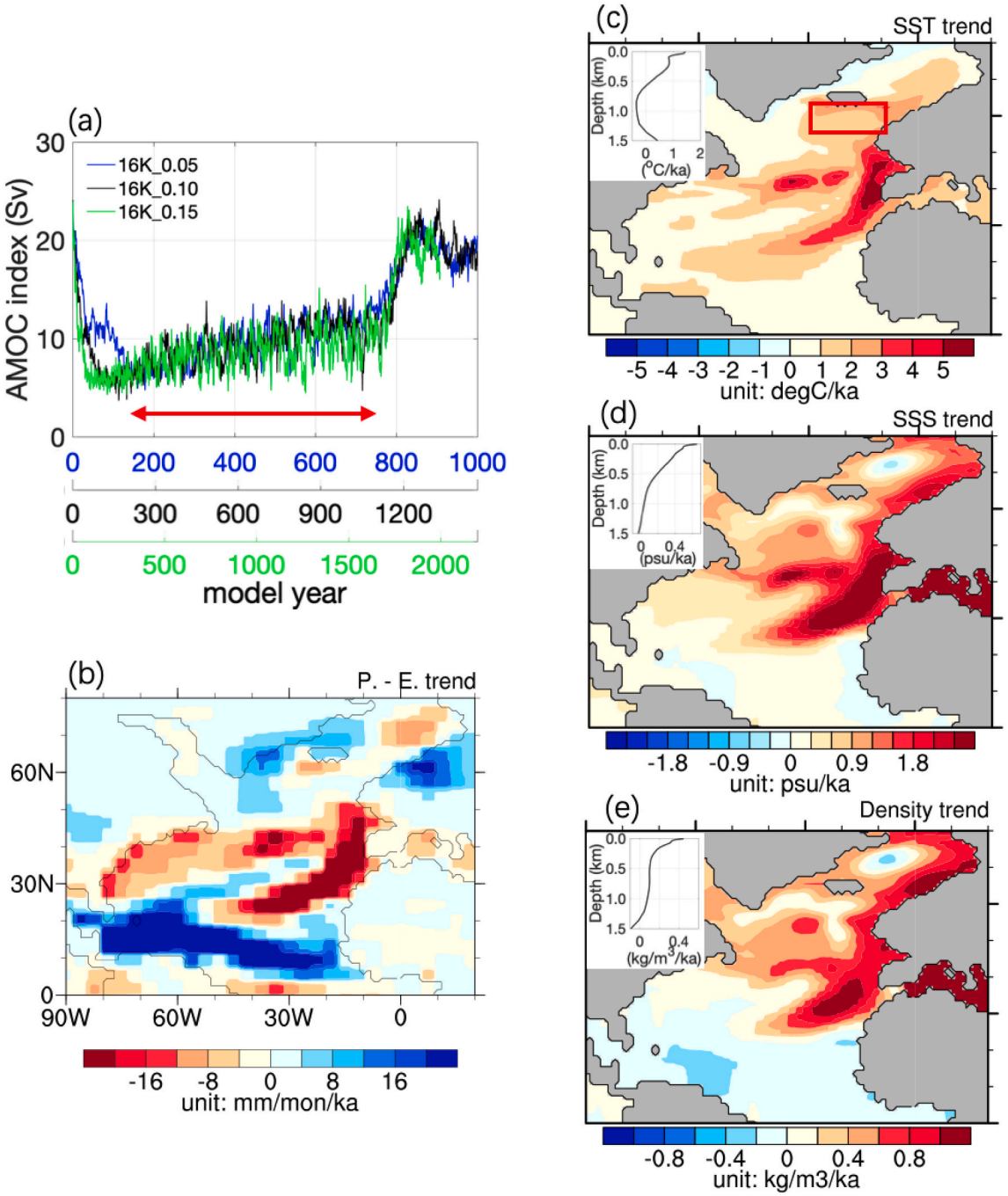

Fig. 6. Trend evolution in the three 16 ka BP experiments with a transient weakening of the AMOC. a) AMOC index (Sv) on the corresponding experiment time scales. The arrow marks the period which is used to calculate the composite trend in b) to e). b) precipitation minus evaporation (mm mon^{-1} ka^{-1}), c) sea surface temperature (SST, $^{\circ}C$ ka^{-1}), d) sea surface salinity (SSS, psu ka^{-1}) and e) sea surface density (kg m^{-3} ka^{-1}). c) to e) contain as an inlet plot the vertical profiles over the index region NENA as defined by the red rectangle in panel c). (For interpretation of the references to colour in this figure legend, the reader is referred to the web version of this article.)

for the rapid AMOC amplification. In section 3.3 we examine the effect of terrestrial ice decline on the AMOC sensitivity to deglacial meltwater flux.

3.1. Mechanism of AMOC recovery

In the three hosing experiments 16K_0.05, 16K_0.10, and 16K_0.15, the AMOC recovers from weak to strong (Fig. 4). The duration of the weak AMOC phase is longer for a stronger MWF and an abrupt amplification process takes place after more than 1500 years in experiment 16K_0.15, which has the strongest sub-critical MWF for the rapid AMOC amplification. All three experiments have an extended phase of gradual AMOC increase prior to the abrupt transition in common. Fig. 6 shows the composite trend analysis of different variables in the gradual phase of these experiments. At the sea surface, a background warming (~1 °C ka^{-1}) decreases the surface water density in the northeastern North Atlantic (NENA, the main convection sites) (Fig. 6c). This strengthens the vertical stratification thermally and stabilizes a weak AMOC. However, at the same time the local sea surface salinity (SSS) has an increasing trend of 0.07 psu ka^{-1}, which counteracts the thermal effect and increases the surface water density (0.5 kg m^3 ka^{-1}) (Fig. 6d,e). Similarly, the subsurface layer density also increases, but with a slower trend than the surface (Fig. 6e inset). This vertical contrast in the rate of water density change highlights the importance of a de-stratification via surface salinization. Especially the simulated southward-shifted ITCZ during the initial AMOC weakening during the first 200 years of hosing are instrumental to increase salinity in the western subtropical North Atlantic (WSNA, 60 –90° W, 10 –30° N) by an increased moisture transport across Central America (Zhang et al., 2017). Since the AMOC is not completely stagnant, the salty WSNA water masses are transported northwards to the North Atlantic deep-water formation areas. This increases the SSS in the northern NA, counteracting the freshwater flux and hence promoting an initial AMOC strengthening once the AMOC reaches its weak mode. As a result, enhanced vertical mixing is identified along the extension area of the Gulf Stream, which leads to a local sea surface warming and an increase in sea surface salinity (Fig. 6c, d) by stronger evaporation. This further increases the vertical mixing and the strength of AMOC providing a positive feedback, which is key to explain the AMOC recovery in our MWF experiments. Taking experiment 16K_0.1 as an example (Fig. 7), salinity is rising in the upper 2000 m of the water column in the North Atlantic, with the most pronounced salinity increase at the surface (Fig. 7a). Consideration of the meridional freshwater transport (MFT), the overturning component of the northward freshwater transport in the Atlantic Ocean (cf. Lohmann, 2003), indicates that northward salinity across 43°N (i.e., the latitude between Gulf Stream extension and sea ice cover) is rising along with the AMOC strengthening until the AMOC amplifies to the strong mode (Fig. 7b).

During the abrupt recovery phase, the preceding ~600 year phase of gradual warming (Fig. 7c) at water depths below ~1500 m plays an important role. As AMOC weakens, a reduced vertical mixing slows down the heat exchange between the cold sea surface and warmer subsurface, leading to a gradual heat accumulation with a maximum temperature increase at ~2000 m. This warming effect on density is not strong enough to overcome the in-situ freshening at the sea surface to generate a destabilization of the stratification. However, when the warm water masses are ventilated to the sea surface, they promote the surface warming, sea-ice retreat and vertical mixing. Given that the core of this warming is at ~2000 m water depth, this positive feedback works only when the strength of the AMOC reach a certain level that enable the water masses to be ventilated to the surface. Hence, this becomes a particularly important positive feedback once the AMOC transition has started (Fig. 7d).

3.2. CO_2 effect on AMOC recovery threshold

From 16 ka BP to the onset of the B/A, the maximum MWF is 0.21 Sv at 15.2 ka. As shown in Fig. 4, this amount of MWF is so strong that the AMOC remains in the weak mode throughout simulation 16K_0.21. In

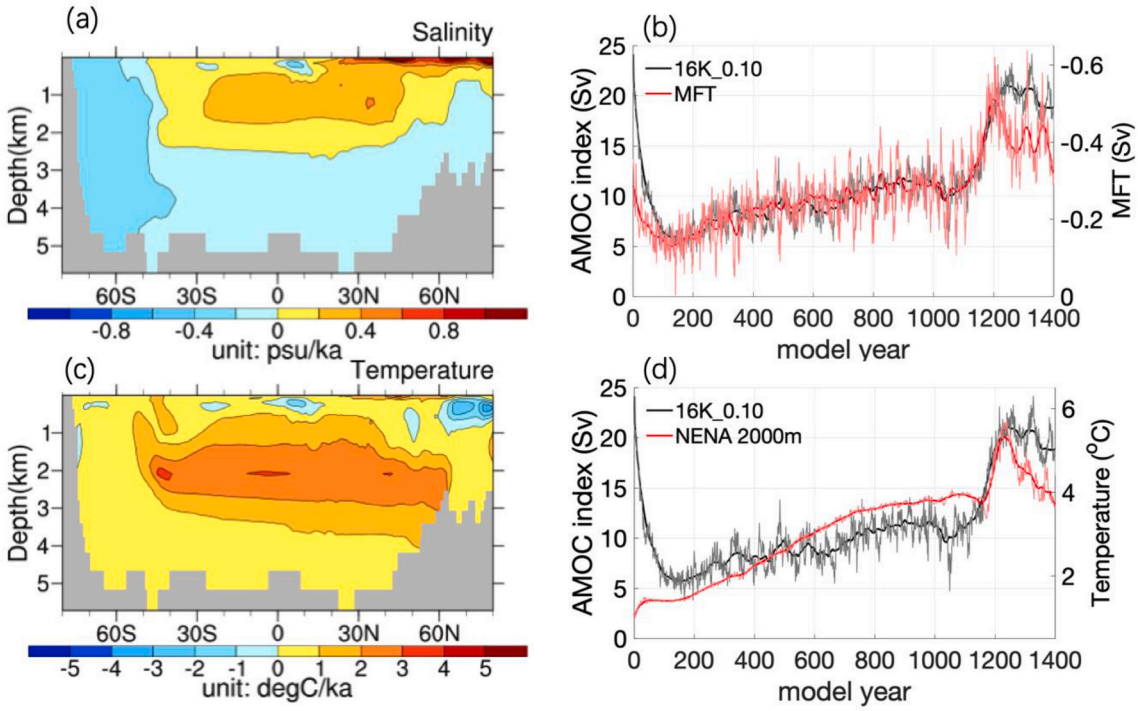

Fig. 7. Trend evolution in experiment 16K_0.1 between model year 200 to 1100. Zonal mean trends in the Atlantic Ocean for a) salinity (psu ka^{-1}) and b) temperature (°C ka^{-1}). c) Time evolution of AMOC index (Sv, black) and MFT in the upper AMOC brunch at 43°N (Sv, red). d) The subsurface (2000 m) temperature (°C, red) evolution averaged in the NENA area. Bold lines in b) and d) represent 50 yr running-mean values. (For interpretation of the references to colour in this figure legend, the reader is referred to the web version of this article.)

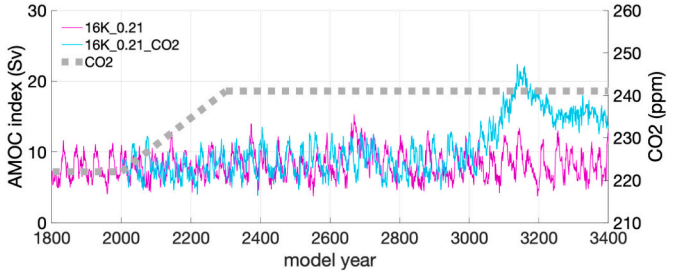

Fig. 8. Time evolution of the AMOC index (Sv) for experiments 16K_0.21 and 16K_0.21_CO2 in response to prescribed atmospheric CO_2 changes (dashed grey line). CO_2 gradually increases from 222 to 241 ppm in the first 300 years in 16K_0.21_CO2. Experiment 16K_0.21_CO2 starts from model year 2000 of 16K_0.21.

experiment 16K_0.21_CO2, we apply a gradual CO_2 increase from 222 ppm to 241 ppm in 300 years, based on simulation 16K_0.21, to test whether a CO_2 rise can trigger the deglacial AMOC recovery. As shown in Fig. 8, an abrupt transition takes place ~1000 years after CO_2 starts to rise. During the gradual phase prior to the abrupt AMOC amplification changes in the MFT across 43°N are similar in both experiments (Fig. 9a). However, the simulated temperature trends in NENA reveal fundamental differences (Fig. 9b). Notably, the temperature trend is positive at all depth levels in in our CO_2 experiment 16K_0.21_CO_2. In contrast the upper ~800 m in our fixed CO_2 experiment 16K_0.21 are characterized by a cooling trend. Furthermore, subsurface temperatures below ~200 m in 16K_0.21_CO_2 show a stronger trend throughout all depth levels of the weakened NADW-cell. The resulting sub-surface warming in the northern North Atlantic (Fig. 9c) leads to an increasing temperature inversion as a key driver of vertical water mass destratification in NENA.

Approximately 1000 years after the start of the CO_2 rise in experiment 16K_0.21_CO2 the stratification at the convection sites breaks down, and the AMOC recovers. From the difference in surface salinity in the last 100 years of the two experiments (Fig. 9d), it can be seen that after the recovery of the AMOC in the 16K_0.21_CO2 experiment, the SSS in the North Atlantic is larger than in the same interval of the 16K_0.21 experiment. The difference is concentrated at the Gulf Stream extension area and North-Eastern Atlantic. Although the timing of a specific meltwater chronology relative to the CO_2 increase might be different, the comparison of the two experiments clearly reveals that a weak AMOC is more likely to recover from HS1 for a higher atmospheric CO_2 concentration.

3.3. Ice Sheet changes and AMOC meltwater sensitivity

So far, we found that the deglacial ice decline generates an AMOC weakening and that under the influence of deglacial meltwater in experiment 16K_0.21 the AMOC resides in a weaker state without any sign of an abrupt AMOC amplification, unless atmospheric CO_2 increases to B/A levels.

To narrow the meltwater flux threshold that controls the abrupt AMOC behavior we perform experiment 16K_0.1_0.2_grad. In this experiment, based on simulation 16K_0.1 we gradually increase the meltwater flux from 0.1 to 0.2 Sv in 1000 years (Fig. 10a). Experiment

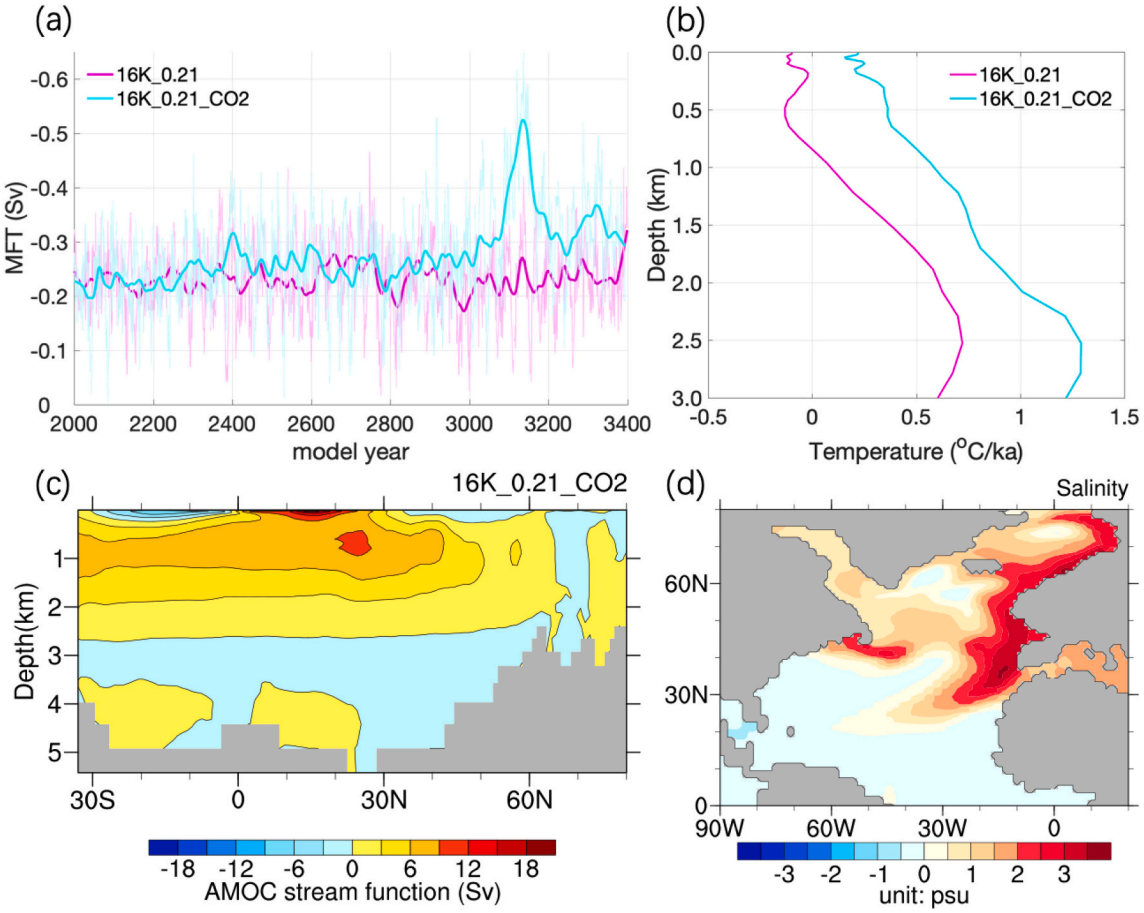

Fig. 9. Experiment characteristics in 16K_0.21 and 16K_0.21_CO2. a) Time evolution of the MFT in the upper brunch of the AMOC at 43°N (Sv), b) vertical temperature profile trends in NENA (cf. Fig. 6c) c) Atlantic stream function in 16K_0.21_CO2 averaged between 2800 and 2900 model years, d) SSS (psu) difference (16K_0.21_CO2 minus 16K_0.21) averaged between model years 3300–3400. Bold solid lines in a) are 50 yr running mean values.

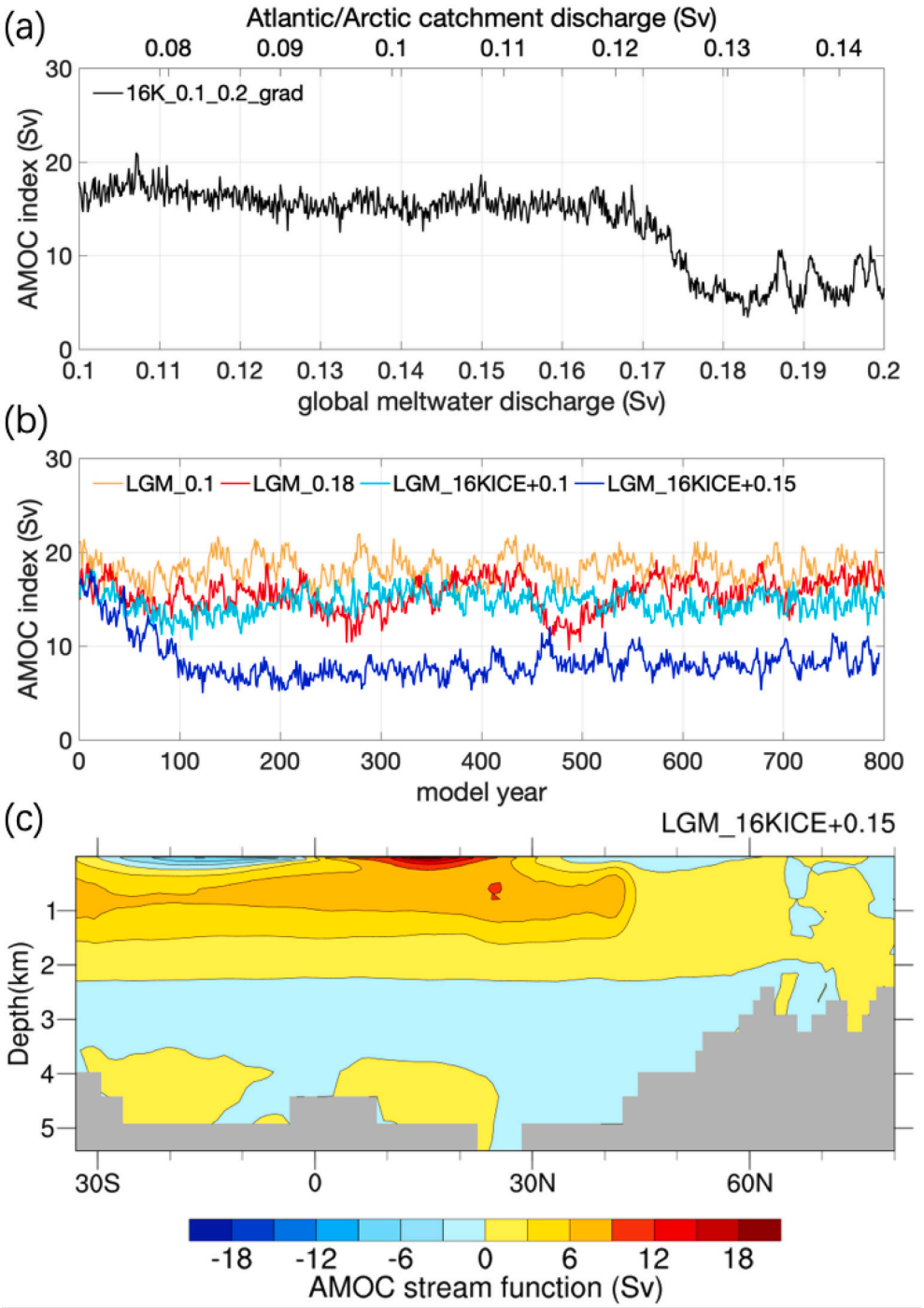

Fig. 10. The time evolution of AMOC index (Sv) in experiment 16K_0.1_0.2_GRAD with a gradual increase of deglacial meltwater discharge from 0.1 to 0.2 Sv based on pattern of MWF2 is shown in panel a). Panel b) shows AMOC changes in the experiments with constant discharge for LGM conditions (LGM_0.1 and LGM_0.18) and LGM conditions, but with reduced ice levels representative of 16 ka (LGM_16KICE+0.1 and LGM_16KICE+0.1). The AMOC stream function (cf. Fig. 5) averaged for the last 100 years in LGM_16KICE+0.15 is shown in panel c).

16K_0.1_0.2_grad shows that the strong to weak AMOC transition is excited for fluxes greater than ~0.17 Sv under full 16 ka conditions. Based on this threshold specification we test the impact of ice sheet changes on the AMOC sensitivity. In experiment LGM_0.18 we apply a MWF larger than the detected threshold under 16 ka conditions, but for full LGM conditions. This experiment shows that the resulting AMOC is stronger (Fig. 10b) than under 16 ka conditions with the same MWF (Fig. 10a), revealing a less sensitive LGM AMOC. Together with our knowledge from the previous section that rising CO_2 can transform a super-critical to a sub-critical MWF perturbation, this result tends to indicate that a larger ice sheet results in a less sensitive AMOC to meltwater fluxes. To further pinpoint the role of declining ice sheets in this sensitivity modulation we perform experiment LGM_16KICE+0.15. In this experiment only the 16 ka ice sheet configuration replaces LGM ice sheet conditions and a MWF of 0.15 Sv is applied (i.e. smaller than the threshold value under 16 ka conditions). This experiment reveals a relatively high sensitivity to deglacial MWF with an AMOC weakening of ~10 Sv (Fig. 10b). The reduction and the resulting AMOC (Fig. 10c) largely resemble the characteristics in experiment 16K_0.21 (Figs. 4 and 5g) in spite of the weaker MFW in LGM_16KICE+0.15. The higher AMOC sensitivity is linked to changes in the westerlies and zonal wind stress (cf. Zhang et al., 2014) that favors enhanced sea ice export to the northeastern North Atlantic. This causes weaker open ocean ventilation and a weaker NADW-cell in experiment LGM_16KICE than in the LGM simulation (Fig. 5a, b) and LGM_16KICE being more susceptible to MWF.

4. Discussion and conclusions

The sequence and dynamics of abrupt deglacial events including the LGM-HS1-B/A has been a source of debate. With respect to the HS1-B/A transition our results are consistent with a growing number of studies that identify a gradual deglacial warming as a cause of an abrupt AMOC increase (e.g., Knorr and Lohmann, 2007; Ganopolski and Roche, 2009; Zhang et al., 2017; Obase and Abe-Ouchi, 2019), without the necessity to invoke a cessation of North Atlantic meltwater fluxes as a trigger for the B/A (e.g. He et al., 2013; Liu et al., 2009; Menviel et al., 2011). Our results also suggest that the MWF magnitude to attain and sustain a weak HS type AMOC is modulated by the deglacial ice decline and CO_2 increase (Zhu et al., 2014; Galbraith and de Lavergne, 2019; Klockmann et al., 2016). More specifically, deglacial land ice decline leads to an increased AMOC sensitivity to MWF. Vice versa, a CO_2 rise decreases this sensitivity. Hence, the increased AMOC sensitivity to meltwater for smaller ice sheets might be an alternative key player contributing to a weak HS1-type AMOC without the necessity to have a corresponding meltwater increase. Vice versa, increasing atmospheric CO_2 can lead to abrupt AMOC recovery at the end of HS1 without invoking a corresponding meltwater decrease. Such a framework is complementary to structural changes in the AMOC by CO_2 and ice height changes (Zhang et al., 2014, 2017) that sensitively depend on the interplay of changes in both control factors. Nevertheless, we highlight here that that neither a freshwater contribution (e.g. 19 ka MWP) to a weak AMOC during HS1 nor a temporal reduction in freshwater just prior to an AMOC amplification at the onset of the B/A can be ruled out as contributing to AMOC changes into and out-off HS1. For further discussion on the interaction of meltwater and stability changes on AMOC variability during deglaciations we refer to Barker and Knorr (2021).

In summary we conducted a set of sensitivity experiments using boundary conditions of LGM and 16 ka based on state-of-the art ice sheet and freshwater reconstructions from GLAC-1D (Tarasov et al., 2012). In the experiments without freshwater perturbation, a relatively strong AMOC state is simulated for 16 ka background conditions. The AMOC strength for 16 ka without meltwater perturbation is only slightly weaker than for the LGM and a meltwater perturbation is required to induce and maintain a weaker HS-type AMOC. The MWF threshold for AMOC transition is dependent on the background climate conditions in our experiments. Notably, rising CO_2 increases the threshold, while deglacial ice decline increases the sensitivity of the AMOC to deglacial meltwater.

For 16 ka conditions, a weaker HS-type circulation can be simulated for meltwater fluxes within the range of reconstructions for HS1. Persistent meltwater input below a critical magnitude only causes a temporal weakening of the AMOC, followed by a fast recovery to a strong AMOC state. A local increase in salinity by increasing northward salinity transport gradually strengthens the AMOC. During the weaker phase, heat is accumulated in intermediate water depth in the North Atlantic Ocean, which ultimately leads to an unstable vertical density profile and an abrupt recovery of AMOC. Such a thermal mechanism has been identified by various types of models and data (e.g., Rühlemann et al., 2004; Knorr and Lohmann, 2007; Kim et al., 2012; Li and Born, 2019; Lohmann et al., 2020). It appears that the subsurface warming in conjunction with an increase in surface salinity leads to an unstable weak AMOC state with a subsequent B/A-type warming during the last deglaciation. We find that the destabilizing feedback depends on the AMOC background strength. In future studies, we will analyze the sequence of deglacial events in climate model setups using interactive ice sheets (e.g., Barbi et al., 2014).

Finally, our findings highlight the importance of well-constrained (within the constraints of limited paleo data) ice sheet/sea level reconstructions for earlier glacial terminations to compare previous deglaciations to Termination 1 and to better understand the rather exceptional early timing of the AMOC recovery at the B/A during the last deglaciation.

Declaration of Competing Interest

The authors declare that they have no known competing financial interests or personal relationships that could have appeared to influence the work reported in this paper.

Acknowledgments

We thank the Max Planck Institute in Hamburg (Germany) for making the COSMOS model available to us. The standard model code of the COSMOS version COSMOS-landveg r2413 (2009) is available upon request from the Max Planck Institute for Meteorology in Hamburg (https://www.mpimet.mpg.de). We acknowledge financial support from the Helmholtz Postdoc Program (PD-301), PACES and REKLIM through the Helmholtz association, as well as from PalMod (01LP1504A and 01LP1915A) through the German Federal Ministry of Education and Research. Computational resources were made available by the infrastructure and support of the computing center of the Alfred Wegener Institute in Bremerhaven and the DKRZ in Hamburg, Germany. Support by the Open Access Publication Funds of Alfred-Wegener-Institut Helmholtz- Zentrum für Polar- und Meeresforschung is acknowledged. We thank the reviewers for their insightful comments and constructive suggetsions.

References

Abelmann, A., et al., 2015. The seasonal sea-ice zone in the glacial Southern Ocean as a carbon sink. Nat. Commun. 6, 1–13.
Banderas, R., Alvarez-Solas, J., Robinson, A., Montoya, M., 2015. An interhemispheric mechanism for glacial abrupt climate change. Clim. Dyn. 44, 2897–2908.
Barbi, D., Lohmann, G., Grosfeld, K., Thoma, M., 2014. Ice sheet dynamics within an Earth system model: coupling and first results on ice stability and ocean circulation. Geosci. Model Dev. 7, 2003–2013. https://doi.org/10.5194/gmd-7-2003-2014.
Bard, E., Rostek, F., Turon, J.L., Gendreau, S., 2000. Hydrological impact of Heinrich events in the subtropical Northeast Atlantic. Science 289, 1321–1324.
Barker, S., Knorr, G., 2007. Antarctic climate signature in the Greenland ice core record. Proc. Natl. Acad. Sci. U. S. A. 104, 17278–17282.
Barker, S., Knorr, G., 2021. Millennial scale feedbacks determine the shape and rapidity of glacial termination. Nat. Commun. 12, 2273. https://doi.org/10.1038/s41467-021-22388-6.
Barker, S., et al., 2011. 800,000 years of abrupt climate variability. Science 334, 347–351.
Barker, S., et al., 2019. Early interglacial legacy of deglacial climate instability. Paleoceanogr. Paleoclimatol. 34, 1455–1475. https://doi.org/10.1029/2019PA003661.
Bereiter, B., Eggleston, S., Schmitt, J., Nehrbass-Ahles, C., Stocker, T.F., Fischer, H., Kipfstuhl, S., Chappellaz, J., 2015. Revision of the EPICA Dome C CO2 record from 800 to 600kyr before present. Geophys. Res. Lett. 42, 542–549. https://doi.org/10.1002/2014GL061957.
Berger, A., 1978. Long-term variations of daily insolation and Quaternary climatic changes. J. Atmos. Sci. 35, 2362–2367.
Böhm, E., et al., 2015. Strong and deep Atlantic meridional overturning circulation during the last glacial cycle. Nature 517, 73–76.
Briggs, R.D., Pollard, D., Tarasov, L., 2014. A data-constrained large ensemble analysis of Antarctic evolution since the Eemian. Quat. Sci. Rev. 103, 91–115.
Brovkin, V., Raddatz, T., Reick, C.H., Claussen, M., Gayler, V., 2009. Global biogeophysical interactions between forest and climate. Geophys. Res. Lett. 36 https://doi.org/10.1029/2009GL037543.
Clark, P.U., McCabe, A.M., Mix, A.C., Weaver, A.J., 2004. Rapid rise of sea level 19,000 years ago and its global implications. Science 304, 1141–1144.
Deaney, E.D., Barker, S., Van de Flierdt, T., 2017. Timing and nature of AMOC recovery across termination 2 and magnitude of deglacial CO_2 change. Nat. Commun. 8 https://doi.org/10.1038/NCOMMS14595.
Denton, G.H., et al., 2010. The last glacial termination. Science 328, 1652–1656. https://doi.org/10.1126/science.1184119.
Dima, M., Lohmann, G., Knorr, G., 2018. North Atlantic versus global control on Dansgaard-Oeschger events. Geophys. Res. Lett. 45, 12,991–12,998. https://doi.org/10.1029/2018GL080035.
Galbraith, E., de Lavergne, C., 2019. Response of a comprehensive climate model to a broad range of external forcings: relevance for deep ocean ventilation and the development of late Cenozoic ice ages. Clim. Dyn. 52, 653–679.
Ganopolski, A., Roche, D.M., 2009. On the nature of lead-lag relationships during glacial-interglacial climate transitions. Quat. Sci. Rev. 28, 3361–3378. https://doi.org/10.1016/j.quascirev.2009.09.019.
Gong, X., Knorr, G., Lohmann, G., Zhang, X., 2013. Dependence of abrupt Atlantic meridional ocean circulation changes on climate background states. Geophys. Res. Lett. 40, 3698–3704.

He, F., Shakun, J.D., Clark, P.U., Carlson, A.E., Liu, Z., Otto-Bliesner, B.L., Kutzbach, J.E., 2013. Northern Hemisphere forcing of Southern Hemisphere climate during the last deglaciation. Nature 494, 81–85.
Hemming, S.R., 2004. Heinrich events: massive late Pleistocene detritus layers of the North Atlantic and their global climate imprint. Rev. Geophys. 42.
Hibler III, W., 1979. A dynamic thermodynamic sea ice model. J. Phys. Oceanogr. 9, 815–846.
Hossain, A., Knorr, G., Lohmann, G., Stärz, M., Jokat, W., 2020. Simulated thermohaline fingerprints in response to different Greenland-Scotland Ridge and Fram Strait subsidence histories. Paleoceanogr. Paleoclimatol. 35 e2019PA003842.
Huang, X., Stärz, M., Gohl, K., Knorr, G., Lohmann, G., 2017. Impact of Weddell Sea shelf progradation on Antarctic bottom water formation during the Miocene. Paleoceanography 32. https://doi.org/10.1002/2016PA002987.
Imbrie, J., et al., 1993. On the structure and origin of major glaciation cycles 2. The 100,000-year cycle. Paleoceanography 8, 699–735.
Jungclaus, J.H., et al., 2006. Ocean circulation and tropical variability in the coupled model ECHAM5/MPI-OM. J. Clim. 19, 3952–3972.
Jungclaus, J.H., et al., 2010. Climate and carbon-cycle variability over the last millennium. Clim. Past 6, 723–737.
Kim, J.-H., Romero, O.E., Lohmann, G., Donner, B., Laepple, T., Haam, E., Damsté, J.S.S., 2012. Pronounced subsurface cooling of North Atlantic waters off Northwest Africa during Dansgaard-Oeschger interstadials. Earth Planet. Sci. Lett. 339-340, 95–102.
Klockmann, M., Mikolajewicz, U., Marotzke, J., 2016. The effect of greenhouse gas concentrations and ice sheets on the glacial AMOC in a coupled climate model. Clim. Past 12, 1829–1846.
Klockmann, M., Mikolajewicz, U., Marotzke, J., 2018. Two AMOC states in response to decreasing greenhouse gas concentrations in the coupled climate model MPI-ESM. J. Clim. 31, 7969–7984.
Knorr, G., Lohmann, G., 2003. Southern Ocean origin for the resumption of Atlantic thermohaline circulation during deglaciation. Nature 424, 532–536. https://doi.org/10.1038/nature01855.
Knorr, G., Lohmann, G., 2007. Rapid transitions in the Atlantic thermohaline circulation triggered by global warming and meltwater during the last deglaciation. Geochem. Geophys. Geosyst. 8 https://doi.org/10.1029/2007GC001604.
Knorr, G., Lohmann, G., 2014. Climate warming during Antarctic ice sheet expansion at the Middle Miocene transition. Nat. Geosci. 7, 376–381.
Knorr, G., et al., 2021. A salty deep ocean as a prerequisite for glacial termination. Nature Geosci. 14, 930–936. https://doi.org/10.1038/s41561-021-00857-3.
Knorr, G., Butzin, M., Micheels, A., Lohmann, G., 2011. A warm Miocene climate at low atmospheric CO_2 levels. Geophys. Res. Lett. 38.
Köhler, P., Nehrbass-Ahles, C., Schmitt, J., Stocker, T.F., Fischer, H., 2017. A 156 kyr smoothed history of the atmospheric greenhouse gases CO2, CH4, and N2O and their radiative forcing. Earth Syst. Sci. Data 9, 363–387.
Li, C., Born, A., 2019. Coupled atmosphere-ice-ocean dynamics in Dansgaard-Oeschger events. Quat. Sci. Rev. 203, 1–20. https://doi.org/10.1016/j.quascirev.2018.10.031.
Liu, Z., et al., 2009. Transient simulation of last deglaciation with a new mechanism for Bølling-Allerød warming. Science 325, 310–314.
Lohmann, G., 2003. Atmospheric and oceanic freshwater transport during weak Atlantic overturning circulation. Tellus 55 A, 438–449.
Lohmann, G., Schulz, M., 2000. Reconciling Bølling warmth with peak deglacial meltwater discharge. Paleoceanography 15 (5), 537–540.
Lohmann, G., Butzin, M., Eissner, N., Shi, X., Stepanek, C., 2020. Abrupt climate and weather changes across timescales. Paleoceanogr. Paleoclimatol. 35 (9) https://doi.org/10.1029/2019PA003782 e2019PA003782.
Loulergue, L., Schilt, A., Spahni, R., Masson-Delmotte, V., Blu-nier, T., Lemieux, B., Barnola, J.-M., Raynaud, D., Stocker, T.F., Chappellaz, J., 2008. Orbital and millennial-scale features of atmospheric CH4 over the past 800 000 years. Nature 453, 383–386. https://doi.org/10.1038/nature06950.
Marsland, S.J., et al., 2003. The Max-Planck-Institute global ocean/sea ice model with orthogonal curvilinear coordinates. Ocean Model 5, 91–127.
McManus, J.F., Francois, R., Gherardi, J.M., Keigwin, L.D., Brown-Leger, S., 2004. Collapse and rapid resumption of Atlantic meridional circulation linked to deglacial climate changes. Nature 428, 834–837.
Menviel, L., Timmermann, A., Timm, O.E., Mouchet, A., 2011. Deconstructing the last glacial termination: the role of millennial and orbital-scale forcings. Quat. Sci. Rev. 30 (9–10), 1155–1172.
Muglia, J., Schmittner, A., 2015. Glacial Atlantic overturning increased by wind stress in climate models. Geophys. Res. Lett. 42, 9862–9868.
Obase, T., Abe-Ouchi, A., 2019. Abrupt Bølling-Allerød warming simulated under gradual forcing of the last deglaciation. Geophys. Res. Lett. 46, 11,397–11,405. https://doi.org/10.1029/2019GL084675.
Oka, A., Hasumi, H., Abe-Ouchi, A., 2012. The thermal threshold of the Atlantic meridional overturning circulation and its control by wind stress forcing during glacial climate. Geophys. Res. Lett. 39.
Raddatz, T.J., et al., 2007. Will the tropical land biosphere dominate the climate–carbon cycle feedback during the twenty-first century? Clim. Dyn. 29, 565–574.
Raymo, M.E., 1997. The timing of major climate terminations. Paleoceanography 12, 577–585.
Roeckner, E., et al., 2003. The General Circulation Model ECHAM5. Part I: Model Description. Max-Planck-Institute for Meteorology, Hamburg, Germany.
Rühlemann, C., Mulitza, S., Lohmann, G., Paul, A., Prange, M., Wefer, G., 2004. Intermediate depth warming in the tropical Atlantic related to weakened thermohaline circulation: Combining paleoclimate and modeling data for the last deglaciation. Paleoceanography 19, PA1025. https://doi.org/10.1029/2003PA000948.
Schilt, A., Baumgartner, M., Schwander, J., Buiron, D., Capron, E., Chappellaz, J., Loulergue, L., Schüpbach, S., Spahni, R., Fischer, H., Stocker, T.F., 2010. Atmospheric nitrous oxide dur- ing the last 140 000 years. Earth Planet. Sci. Lett. 300, 33–43. https://doi.org/10.1016/j.epsl.2010.09.027.
Sherriff-Tadano, S., Abe-Ouchi, A., Yoshimori, M., Oka, A., Chan, W.-L., 2018. Influence of glacial ice sheets on the Atlantic meridional overturning circulation through surface wind change. Clim. Dyn. 50, 2881–2903.
Simon, M.H., et al., 2015. Salt exchange in the Indian-Atlantic Ocean Gatewaysince the Last Glacial Maximum: A compensating effect between Agulhas Current changes. Paleoceanography 30, 1318–1327. https://doi.org/10.1002/2015PA002842.
Stepanek, C., Samakinwa, E., Knorr, G., Lohmann, G., 2020. Contribution of the coupled atmosphere–ocean–sea ice–vegetation model COSMOS to the PlioMIP2. Clim. Past 16, 2275–2323. https://doi.org/10.5194/cp-16-2275-2020.
Stocker, T., 2000. Past and future reorganizations in the climate system. Quat. Sci. Rev. 19, 301–319.
Tarasov, S., Dyke, Arthur S., Neal, Radford M., Peltier, W.R., 2012. A data-calibrated distribution of deglacial chronologies for the north American ice complex from glaciological modeling. Earth Planet. Sci. Lett. 315, 30–40.
Tarasov, L., Hughes, A., Gyllencreutz, R., Lohne, O.S., Mangerud, J., Svendsen, J.I., 2014. The global GLAC-1c deglaciation chronology, melwater pulse 1-a, and a question of missing ice. In: IGS Symposium on Contribution of Glaciers and Ice Sheets to Sea-Level Change.
Venz, K.A., Hodell, D.A., Stanton, C., Warnke, D.A., 1999. A 1.0 Myr record of glacial North Atlantic intermediate water variability from ODP site 982 in the Northeast Atlantic. Paleoceanography 14, 42–52.
Wei, W., Lohmann, G., 2012. Simulated Atlantic multidecadal oscillation during the Holocene. J. Clim. 25, 6989–7002.
Wei, W., Lohmann, G., Dima, M., 2012. Distinct modes of internal variability in the global meridional overturning circulation associated with the Southern Hemisphere westerly winds. J. Phys. Oceanogr. 42, 785–801.
Zhang, X., Lohmann, G., Knorr, G., Xu, X., 2013. Different ocean states and transient characteristics in last Glacial Maximum simulations and implications for deglaciation. Clim. Past 9, 2319–2333.
Zhang, X., Lohmann, G., Knorr, G., Purcell, C., 2014. Abrupt glacial climate shifts controlled by ice sheet changes. Nature 512, 290–294.
Zhang, X., et al., 2021. Direct astronomical influence on abrupt climate variability. Nature Geosci. 14, 819–826. https://doi.org/10.1038/s41561-021-00846-6.
Zhang, X., Knorr, G., Lohmann, G., Barker, S., 2017. Abrupt North Atlantic circulation changes in response to gradual CO_2 forcing in a glacial climate state. Nat. Geosci. 10, 518–523. https://doi.org/10.1038/ngeo2974.
Zhu, J., Liu, Z., Zhang, X., Eisenman, I., Liu, W., 2014. Linear weakening of the AMOC in response to receding glacial ice sheets in CCSM3. Geophys. Res. Lett. 41, 6252–6258. https://doi.org/10.1002/2014GL060891.